INSTITUTE OF PHYSICS PUBLISHING JOURNAL OF PHYSICS D: APPLIED PHYSICS
J. Phys. D: Appl. Phys. **38** (2005) 2103–2111 doi:10.1088/0022-3727/38/13/005

High-speed quantum dot lasers

S Fathpour, Z Mi and P Bhattacharya

Department of Electrical Engineering and Computer Science, University of Michigan, Ann Arbor, MI 48109-2122, USA

Received 21 December 2004, in final form 24 February 2005
Published 17 June 2005
Online at stacks.iop.org/JPhysD/38/2103

Abstract
The modulation bandwidth of conventional 1.0–1.3 μm self-organized In(Ga)As quantum dot (QD) lasers is limited to ∼6–8 GHz due to hot carrier effects arising from the predominant occupation of wetting layer/barrier states by the electrons injected into the active region at room temperature. Thermal broadening of holes in the valence band of QDs also limits the performance of the lasers. Tunnel injection and p-doping have been proposed as solutions to these problems. In this paper, we describe high-performance In(Ga)As undoped and p-doped tunnel injection self-organized QD lasers emitting at 1.1 and 1.3 μm. Undoped 1.1 μm tunnel injection lasers have ∼22 GHz small-signal modulation bandwidth and a gain compression factor of 8.2×10^{-16} cm^3. Higher modulation bandwidth (∼25 GHz) and differential gain (3×10^{-14} cm^2) are measured in 1.1 μm p-doped tunnel injection lasers with a characteristic temperature, T_0, of 205 K in the temperature range 5–95˚C. Temperature invariant threshold current (infinite T_0) in the temperature range 5–75˚C and 11 GHz modulation bandwidth are observed in 1.3 μm p-doped tunnel injection QD lasers with a differential gain of 8×10^{-15} cm^2. The linewidth enhancement factor of the undoped 1.1 μm tunnel injection laser is ∼0.73 at lasing peak and its dynamic chirp is <0.6 Å at various frequencies and ac biases. Both 1.1 and 1.3 μm p-doped tunnel injection QD lasers exhibit zero linewidth enhancement factor ($\alpha \sim 0$) and negligible chirp (<0.2 Å). These dynamic characteristics of QD lasers surpass those of equivalent quantum well lasers.

1. Introduction

Self-organized quantum dot (QD) lasers have been the subject of extensive study in the last decade and have demonstrated lower threshold current, linewidth enhancement factor and dynamic chirp compared to quantum well (QW) lasers [1–3]. Demonstration of high-speed QD lasers can, therefore, be envisioned as a breakthrough in terms of applications as coherent light sources for 1.0–1.3 μm short-haul local area network (LAN) and metropolitan area network (MAN) 10 Gb s^{-1} communication systems. However, achieving high modulation bandwidths with conventional separate confinement heterostructure (SCH) QD lasers has not been possible [4]. There are unique problems that limit the modulation performance of conventional SCH QD lasers, compared to what is expected from an 'ideal' QD laser with a discrete density of states. First, the inhomogenous linewidth broadening, associated with the stochastic size distribution of the dots, imposes a limit on the performance of QD lasers. More importantly, SCH QD lasers suffer from significant hot-carrier effects and associated gain compression due to the large density of states of the wetting layer and barrier states, compared with that in the QDs [5]. As a result, the conventional devices cannot be modulated at bandwidths above 6–8 GHz [4]. In addition, the hole distribution is thermally broadened into many available states with small energy spacings in QDs and a large injected hole density is required for a large gain in the ground state. This would also decrease the attainable gain and differential gain in conventional QD lasers.

Two unique solutions have been proposed and implemented to overcome these problems in conventional SCH QD lasers: tunnelling injection (TI) and acceptor (p) doping of the dots [6–13]. In the tunnel injection scheme, 'cold carriers' are injected directly into the ground state of the QDs by phonon-assisted tunnelling from an adjacent injector layer and are removed by stimulated emission at approximately the same rate. Therefore, the differential gain of the lasers can be optimized and hot carrier effects are minimized. With p-doping, extra holes are provided at the ground state energy by either direct doping of the dots or by modulation doping in the GaAs

0022-3727/05/132103+09\$30.00 © 2005 IOP Publishing Ltd Printed in the UK

barriers. These extra holes ensure population inversion with less injected holes from the contacts; consequently, the electron population in the dots and their leakage into barrier and waveguide layers is reduced as well.

In this paper, we will first describe the intrinsic characteristics of QD lasers that determine the small-signal modulation bandwidth and the temperature dependence of the threshold current. This is followed by a description of tunnel injection and p-doping in QD lasers and a comparison of the two approaches. We will see that although p-doping is helpful in improving the characteristic temperature, T_0, of QD lasers—especially at 1.3 μm—it does not help in realizing high modulation bandwidth lasers. On the other hand, tunnel injection not only decreases the temperature sensitivity of QD lasers, but also significantly enhances the high frequency response of the devices. Specifically, the properties of 1.1 μm and 1.3 μm QD lasers, in which tunnel injection and p-doping are incorporated, are described. The high-speed modulation characteristics of these devices are described and discussed. Finally, data on chirp and α-factor of these devices are presented. It will be evident that present high-speed QD lasers are promising candidates for applications in MAN and LAN systems.

2. Factors limiting high-speed operation of QD lasers

It is now recognized that the limitations to high-speed modulation of conventional SCH QD lasers is due to the electronic properties of the QDs arising from the nature of self-assembled growth. Due to the large lattice mismatch in the In(Ga)As/GaAs system (> 1.7%), the dots are formed in the Stranski–Krastanow growth mode, where zero-dimensional islands (QDs) are formed on top of a wetting layer (two-dimensional electron-gas), as depicted in figure 1. The QDs and the wetting layer form a coupled electronic system, whose statistics cannot be described by quasi-Fermi equilibrium. Due to the large number of the states in the two-dimensional electron-gas compared to the number of states in the dots, injected carriers predominantly reside in the higher energy

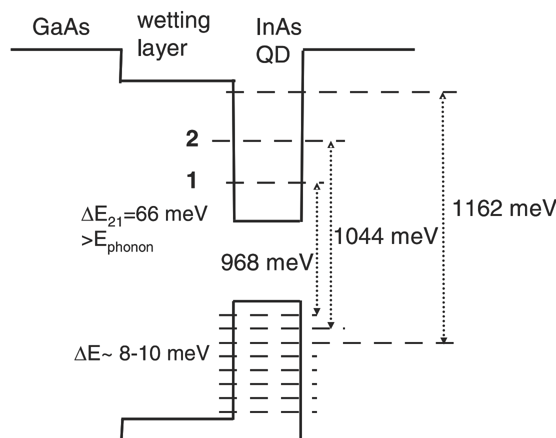

Figure 1. Energy levels of 1.3 μm QDs showing the large energy spacing between the ground and first excited state in the conduction band and many (~10) levels with small spacing (8–10 meV) in the valence band.

states in the wetting layer and QD lasers suffer from this undesired 'hot carrier' effect and associated gain saturation. Differential transmission spectroscopy (DTS) measurements have indeed shown that electrons captured in the wetting layer/barrier states tend to remain there at temperatures above 180 K, i.e. they undergo very slow relaxation to the lasing energy state [14]. Matthews *et al* [5] also observed severe gain saturation in QDs at above 150 K and showed that it can be explained by incomplete population inversion in the ground state of the QDs due to the occupancy of the wetting layer states. The gain saturation leads to low modulation bandwidth. Stated differently, the entropy change of carriers relaxing from the two-dimensional wetting layer states to the zero-dimensional QDs is responsible for the low modulation bandwidths measured in QD lasers [15].

An ideal QD laser should preferably have only one electron and one hole energy level. As shown in figure 1, the inevitable existence of multiple hole energy levels with small energy spacing (8–10 meV) results in thermal broadening of the hole population in energy. Consequently, the ground state hole population is depleted, leading to a decrease in gain. A higher injection of holes, to compensate for this effect, necessitates increased injection of electrons due to requirements of charge neutrality. The excess carriers lead to leakage, non-radiative recombination outside the core, increased threshold current and reduced differential gain.

3. Tunnel injection and acceptor doping in QD lasers

TI and p-doping have been suggested and studied as two promising techniques to solve the hot-carrier related problems in QD lasers [6–13]. Tunnel injection was originally proposed and demonstrated more than a decade ago to reduce hot carrier effects in QW lasers [16–18]. In this scheme, 'cold carriers' are directly injected into the lasing energy state from an adjoining injector layer; thus hot carrier effects can be bypassed and the performance of the lasers would improve. High-performance GaAs- and InP-based QW lasers with high T_0, reduced chirp and improved modulation bandwidths have been reported by our group for a long time [17, 18]. TI, however, is more useful in enhancing the modulation bandwidth of QD lasers. As shown in figure 2(*a*), cold electrons injected into the ground state of the QDs by phonon-assisted tunnelling can by-pass the hot carrier problems associated with the capture of electrons into the wetting layer/barrier energy states. Femtosecond DTS measurement of phonon-assisted tunnelling confirms fast (~1.7 ps) temperature-independent tunnelling times [6]. Tunnelling also decreases carrier radiative recombination in the wetting layer/barrier regions, and based on this Asryan and Luryi theoretically predicted a significant increase of T_0 [10]. We demonstrated a large increase in modulation bandwidth (~15 GHz) in our first tunnel injection QD lasers [19] and as will be seen in the following, the characteristics of our lasers have steadily improved since then.

p-Doping of QD lasers can be achieved by either direct or modulation doping of the dots. As shown in figure 2(*b*) for the modulation doping case, the holes of the p-doped barrier are transferred into the hole ground state with lower energy in the adjacent QD layer; thus, fewer electron–hole pairs are required to be injected from the contacts to compensate for

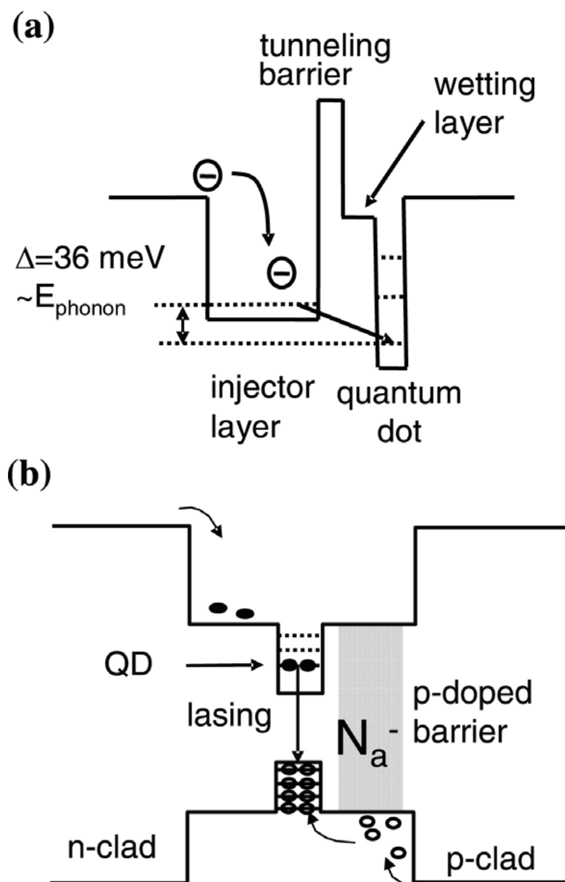

Figure 2. (*a*) Injection of cold carriers into the ground state of the dot by tunnelling from an adjoining injector layer; (*b*) modulation p-doping of the QD barrier in order to increase the gain through the increase of hole ground state occupancy.

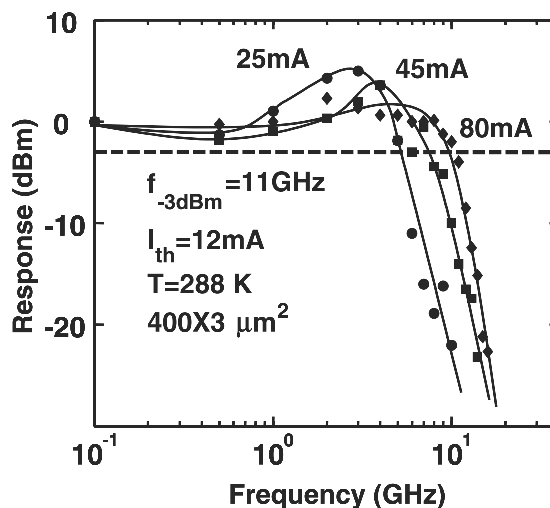

Figure 3. Modulation response of single-mode 1.1 μm p-doped QD SCH laser at different biases with a maximum 3 dB bandwidth of ~11 GHz.

the thermal broadening of the hole distribution. Vahala and Zah predicted an increase of gain in p-doped QW lasers [20], which was followed by the prediction of enhancement of the relaxation oscillation frequency and reduction of linewidth enhancement factor in multi-QW lasers [21]. p-Doping is expected to be more beneficial in QD lasers due to the more pronounced thermal broadening of holes in the valence band with smaller energy spacing in QDs than in QWs. Miyamoto *et al* [7] proposed p-doping for increase of gain and reduction of threshold current. Deppe *et al* have modelled the impact of p-doping on the modulation response and characteristic temperature, T_0, of QD lasers [8] and have experimentally demonstrated T_0 as high as 213 K in p-doped InAs QD lasers [9]. We have measured temperature invariant operation ($T_0 = \infty$) in p-doped 1.3 μm QD SCH lasers and have attributed this result to a significant role of Auger recombination with its unique temperature dependence [12]. However, contrary to theoretical predictions [8], we observed only a slight improvement in modulation bandwidth, from 9 GHz in undoped lasers to 11 GHz in 1.1 μm p-doped lasers with otherwise identical heterostructures. The modulation response of the p-doped lasers is presented in figure 3, from which a differential gain of 6.9×10^{-15} cm^2 is obtained. The low bandwidth can be attributed to the inefficiency of p-doping due to the wetting layer states [22], inadequate enhancement of gain and differential gain, and the increased damping effect of Auger recombination in the modulation response.

These observations confirm that although p-doping may be beneficial in enhancing T_0, tunnel injection appears to be a better approach to achieve high-speed QD lasers. In the following, we present the growth, fabrication and characteristics of state-of-the-art 1.1 and 1.3 μm tunnel injection QD lasers. As will be evident, in some of these devices, both techniques of tunnel injection and p-doping are *simultaneously* incorporated.

4. Growth and fabrication of tunnel injection lasers with p-doping

Three types of tunnel injection lasers are discussed in this work. They are undoped and p-doped 1.1 μm lasers and p-doped 1.3 μm lasers. All the laser heterostructures were grown by molecular beam epitaxy (MBE) on (001) GaAs substrates. The heterostructure of a 1.1 μm InGaAs tunnel injection QD lasers is schematically shown in figure 4(*a*). The wavelength of the dot luminescence peak is controlled by adjusting the InGaAs dot charge during epitaxy. The active region consists of a 95 Å $In_{0.25}Ga_{0.75}As$ injector well, a 20 Å $Al_{0.55}Ga_{0.45}As$ tunnel barrier, and three coupled $In_{0.50}Ga_{0.50}As$ QD layers. The $In_{0.25}Ga_{0.75}As$ injector layer is grown at 450°C and the QD layers are grown at 510°C. The energy separation in the conduction band between the injector layer state and the QD ground state is ~36 meV at room temperature. This energy separation ensures longitudinal optical (LO) phonon-assisted tunnelling from the injector layer to the dot ground states through the AlGaAs barrier. In the p-doped lasers, doping is provided by delta-doping (5×10^{11} cm^{-2}) the 500 Å barrier/waveguide region grown on top of the three layers of coupled QDs. 50 nm of the GaAs waveguide above the three coupled QD layers are p-type doped with beryllium ($N_a = 5 \times 10^{17}$ cm^{-3}), averaging about 20 holes per dot.

Figure 5(*a*) shows the band diagram in the active region of the 1.3 μm p-doped tunnel injection QD laser. All the depicted energy transitions are calculated and design values.

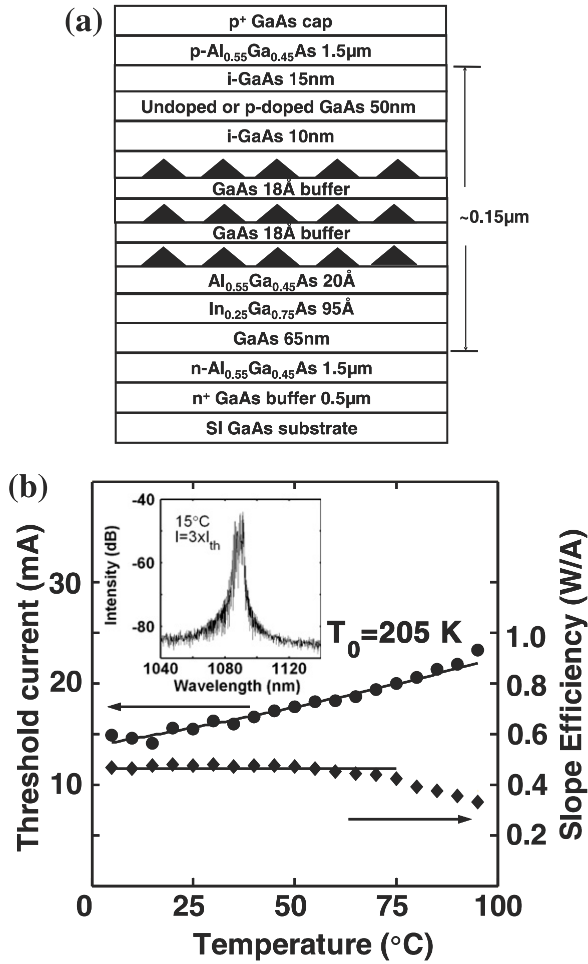

Figure 4. (*a*) Heterostructure schematic of 1.1 μm undoped and p-doped tunnel injection QD lasers; (*b*) variation of the threshold current and slope efficiency of 200 × 3 μm^2 single-mode 1.1 μm p-doped lasers with temperature. The inset shows the output spectrum of the laser at 3 times threshold.

Long wavelength (1.3 μm) tunnel injection QD lasers are more difficult to realize due to the higher misfit-related strains involved in this system. In order to reduce the strain, the design of 1.3 μm QD lasers differs from the 1.1 μm lasers in that electrons tunnel into the first excited states of the dot, instead of the ground state. This eases the alloying requirements of the injected layer. Pump-probe DTS measurements show that the relaxation time from the dot first excited state to the ground state is very small, ~130 fs, if the excited states are filled with electrons, i.e. lasing conditions [23]. One QD layer, which consists of 2.6 ML of InAs capped with 45 Å $In_{0.15}Ga_{0.85}As$, is grown on top of its neighbouring 95 Å $In_{0.27}Ga_{0.73}As$ injection layer. In order to increase the modal gain, five periods of injector/QDs/GaAs buffers are stacked. Compared to the 1.1 μm design, shorter tunnel barriers ($Al_{0.25}Ga_{0.75}As$) are employed to facilitate carrier injection across the SCH region. It has to be noted that carrier lifetimes are long enough to ensure they reach all the five dot layers, as has been shown in 70-layer QD infrared photodetectors by Monte Carlo simulations [24]. As shown in figure 5(*b*), the laser heterostructure exhibits strong photoluminescence (PL) with a narrow linewidth at room temperature. This is an indication of efficient tunnelling due to the selection process of the tunnelling states in the dots.

Mesa-shaped broad area (20–100 μm-wide) and single-mode ridge waveguide lasers (3–5 μm ridge width) were fabricated by standard lithography, wet and dry etching and metallization techniques. 200–2000 μm long lasers were obtained by cleaving. Measurements were made on lasers with as-cleaved facets, as well as, facets with high reflectivity mirrors obtained with the deposition of dielectric distributed Bragg reflectors (DBR).

5. Static characteristics of QD lasers

Light-current (L-I) measurements were made with the devices mounted on a Cu heat-sink, whose temperature was stabilized with a Peltier cooler. Pulsed biased (1 μs, 10 kHz) light-current measurements were performed on 1.1 μm TI-QD p-doped as-cleaved 200 × 3 μm^2 single-mode lasers and as the threshold current versus temperature plot in figure 4(*b*) indicates, $T_0 \sim$ 205 K from 5˚C to 95˚C and slope efficiency of 0.465 W A^{-1} can be extracted for the devices. The inset shows the output spectrum of the device lasing at about 1090 nm. Similarly, the undoped 1.1 μm TI-QD lasers exhibit $T_0 \sim 363$ K for 5˚C $< T <$ 60˚C and a threshold current of 8 mA at 288 K for a 400 × 3 μm^2 device. From the L-I characteristics of undoped TI lasers of varying cavity length, we determine the value of internal quantum efficiency $\eta_i = 85\%$ and cavity loss $\gamma = 8.2\,\text{cm}^{-1}$, by plotting the inverse of differential efficiency, η_d, against cavity length, l. It is evident that the characteristic temperature of TI lasers is much higher than typical values of $T_0 < 100$ K in conventional QD lasers, which is due to efficient (direct) injection of cold carriers into the ground state of QDs, minimal occupation of wetting layer/barrier states, and the consequent reduction in the radiative recombination component of threshold current from these higher energy states.

For the 1.3 μm p-doped TI QD lasers, L-I measurements were performed on devices with 95% high reflectivity mirrors on one facet. The room temperature L-I characteristics of an 800 × 5 μm^2 single-mode laser, with its optical output spectrum, are shown in figure 6(*a*). It is evident that the laser single-mode peak is from the ground state of the dots and is very close to the corresponding PL peak in figure 5(*b*). The value of J_{th} is 180 A cm^{-2} for an 800 μm long cavity. Values of $\eta_i = 71\%$ and cavity loss $\gamma = 6.3\,\text{cm}^{-1}$ were determined for these devices under quasi-CW bias (10% duty cycle) from the η_d^{-1} versus l plot. A differential gain of 9.8×10^{-15} cm^2 is estimated in the devices from the same plot.

The threshold current of a 400 × 5 μm^2 device versus temperature is shown in figure 6(*b*). It is observed that $T_0 = \infty$ in the temperature range of 5–70˚C. This result is similar to our first report on temperature invariant operation of p-doped 1.3 μm QD lasers [12]. As discussed in detail therein, although high T_0 has been predicted and previously reported in p-doped QD lasers [7–9], complete temperature independence of I_{th} may seem unlikely, since the inhomogeneous linewidth broadening of the gain, associated with the stochastic size distribution of self-organized QDs, should limit such ideal performance of QD lasers. The radiative recombination terms in the wetting layers and GaAs barrier/waveguide regions are

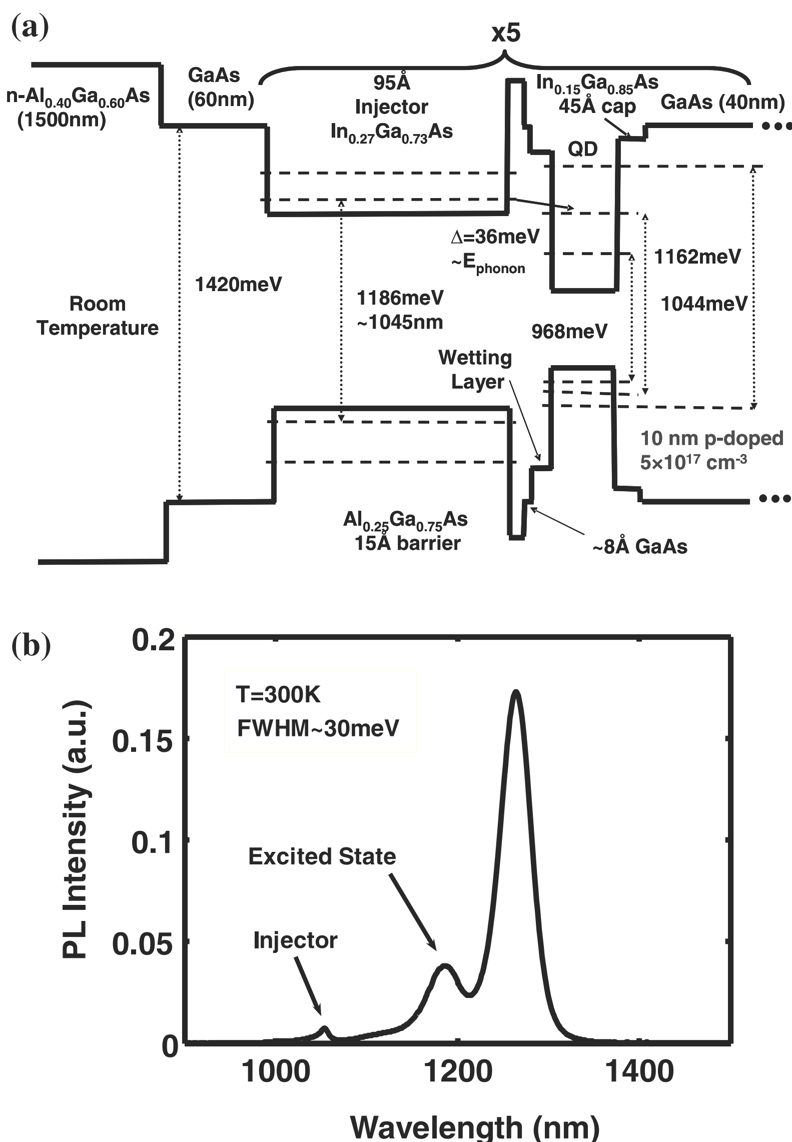

Figure 5. (*a*) The energy band diagram in the active region of 1.3 μm p-doped tunnel injection QD lasers illustrating the phonon-assisted tunnelling from the injector layer into the first excited state; (*b*) room temperature PL spectrum of the heterostructure showing distinct peaks from the dot ground and excited states and the injector layer state.

functions of the Fermi–Dirac distribution, i.e. they contribute to finite T_0, as well. Therefore, a recombination process whose rate decreases with temperature has to be considered in order to explain the experimentally observed $T_0 = \infty$. We have employed a self-consistent model [12] to calculate the various radiative and non-radiative current components in p-doped and undoped lasers and concluded that the zero temperature dependence of the p-doped 1.3 μm QD SCH lasers is due to the significant role of Auger recombination in the devices, and its decrease with temperature according to the temperature dependence of the Auger coefficient [25]. We believe the lower $T_0 = 205$ K in the 1.1 μm p-doped TI lasers is a consequence of the following: (a) the Auger recombination is expected to be lower in higher band gap materials, as confirmed by hydrostatic pressure dependence measurements [26]. Therefore, Auger recombination is less effective in playing the compensating role to achieve high T_0; (b) the conduction and valence band offsets (ΔE_C and ΔE_V) are smaller in 1.1 μm QDs than in longer wavelength 1.3 μm dots. Consequently, the carrier leakage into the barrier/waveguide region is higher in 1.1 μm QDs, which also leads to a lower value of T_0.

6. Small signal modulation response

The small signal modulation response of the lasers was measured with a high-speed photodetector, low-noise amplifier, a HP 8350B sweep oscillator and a HP 8562A electrical spectrum analyser. The modulation response of the undoped 1.1 μm TI-QD laser at room temperature and at different injection currents is shown in figure 7. It is seen that the lasers have a maximum modulation bandwidth, $f_{-3\,\mathrm{dB}}$, of $\sim$22 GHz at a bias of 125 mA. By plotting the resonance frequency versus $(I - I_{\mathrm{th}})^{1/2}$ a modulation efficiency of $\sim$1.7 GHz mA$^{-1/2}$ is derived in these lasers. A differential gain, $\mathrm{d}g/\mathrm{d}n = 2.7 \times 10^{-14}$ cm^2 in these devices is derived from the measured modulation efficiency and a calculated

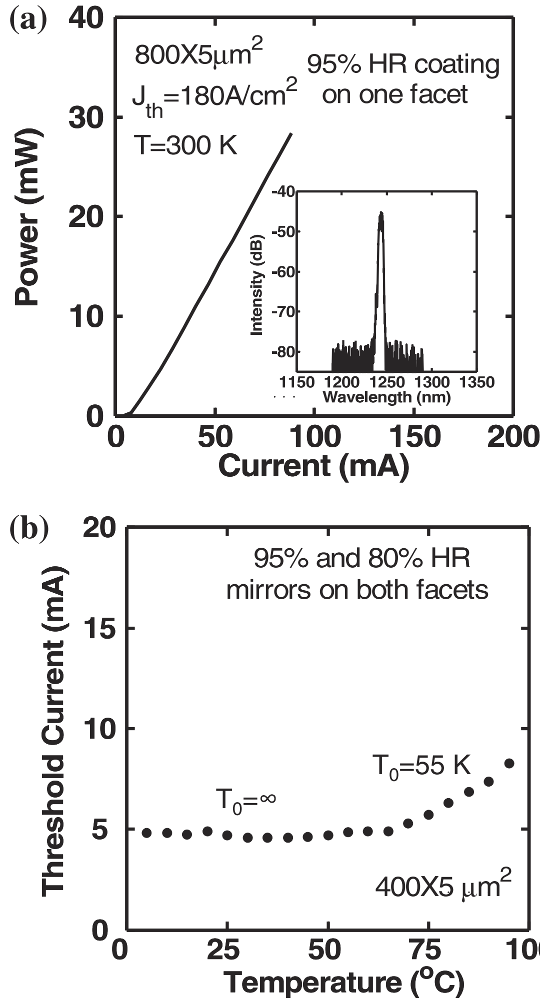

Figure 6. (*a*) Pulsed light-current characteristics of 1.3 μm p-doped tunnel injection single mode QD lasers at room temperature. The inset shows the output spectrum; (*b*) variation of threshold current of the 1.3 μm lasers with temperature.

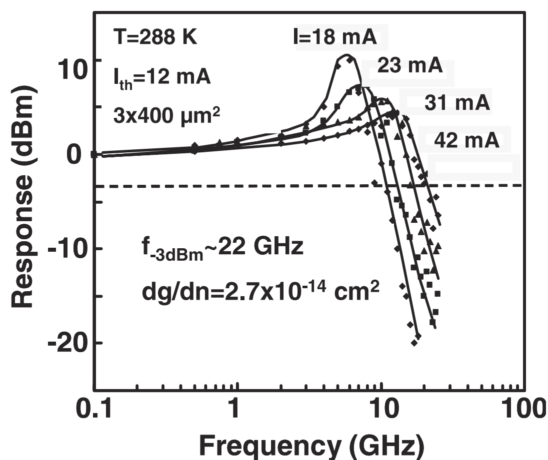

Figure 7. Modulation response of single-mode 1.1 μm undoped tunnel injection QD lasers at different biases at 15°C.

optical confinement factor of $\Gamma = 2.5 \times 10^{-3}$. From the damping factor of the best fit to the modulation response, a gain compression factor, $\varepsilon = 8.2 \times 10^{-16}$ cm^3 is also obtained for these devices.

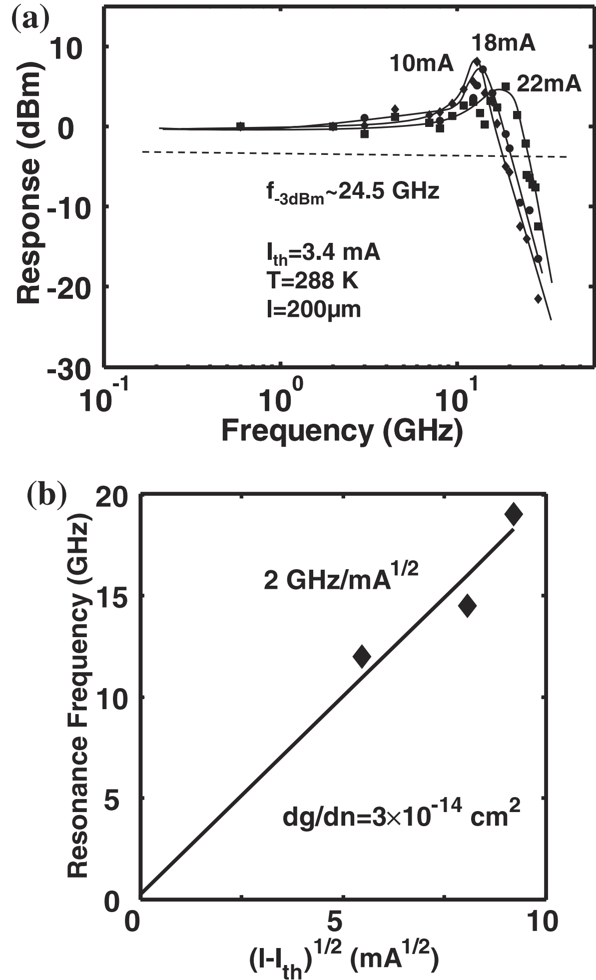

Figure 8. (*a*) Modulation response of single-mode 1.1 μm p-doped QD tunnel injection lasers at different biases; (*b*) resonance frequency of the lasers versus $\sqrt{I - I_{\mathrm{th}}}$.

The modulation response for the 1.1 μm p-doped TI QD lasers is shown in figure 8(*a*). The measurements were made under pulsed bias. The maximum $f_{-3\,\mathrm{dB}}$ measured for an injection bias of $6.7 \times I_{\mathrm{th}}$ is $\sim$24.5 GHz, which is higher than the undoped sample and is indeed the highest modulation bandwidth reported to date in any QD laser. The resonance frequency of the devices is plotted versus $(I - I_{\mathrm{th}})^{1/2}$ in figure 8(*b*), from which a modulation efficiency and differential gain of 2 GHz mA$^{-1/2}$ and 3×10^{-14} cm^2, respectively, are derived. The corresponding extracted gain compression factor of the lasers is $\varepsilon = 4 \times 10^{-16}$ cm^3. All these parameters show improvement compared to the undoped samples, which may be attributed to the slight impact of p-doping in the modulation characteristics of QD lasers. As briefly discussed in section 3, we have also observed a few gigahertz enhancement of modulation bandwidth upon p-doping (from 9 to 11 GHz) in conventional 1.1 μm SCH lasers, which is due to the slight increase of gain and differential gain by the extra holes provided from the doped barriers.

Figure 9 presents the modulation response characteristics of a single-mode $400 \times 3\,\mu$m^2 p-doped 1.3 μm TI QD lasers. A maximum 3 dB modulation bandwidth of 11 GHz is measured in these devices at 45 mA. A modulation efficiency

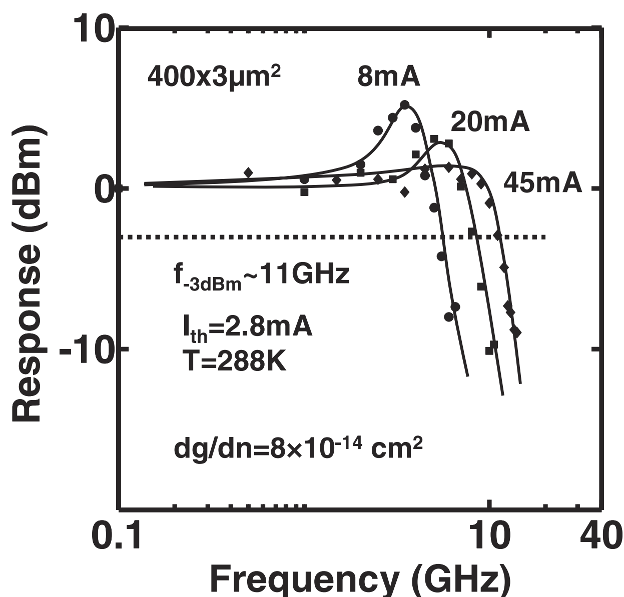

Figure 9. Modulation response of single-mode 1.3 μm p-doped QD tunnel injection lasers at different biases at 15˚C.

of 1.1 GHz mA$^{-1/2}$ and a differential gain of 8×10^{-15} cm^2 are extracted, the latter of which is close to the estimation of the figure from the dc measurements presented before. We can speculate the following as a reason for the lower bandwidths observed in 1.3 μm TI QD lasers compared to that measured in 1.1 μm TI QD lasers (figures 7 and 8). As discussed before, very fast tunnelling time constant and relaxation times from the dot excited states to the ground state have been measured by DTS [6, 23]. Therefore, the 1.3 μm tunnel injection lasers are most probably not limited by relaxation and tunnelling times. The modal gain of a QD laser is proportional to dot density (fill factor) and density of states, of which the latter is inversely proportional to the average volume of a single dot. The average volume of the 1.3 μm dots is about a factor of 2 larger and the dot density is usually lower compared to 1.1 μm QDs. These geometrical differences translate to lower gain and differential gain in 1.3 μm lasers.

7. Dynamic properties: chirp and α-factor

The modulation characteristics of tunnel injection lasers presented in the previous section indicate that these devices have enormous potential for high-speed fibre optic communication LAN and MAN systems. Therefore, we have also studied important dynamic figures of merit for such applications in the present lasers, namely, linewidth enhancement factor, α, and dynamic chirp. The α-factor is a critical parameter in semiconductor lasers, since the laser linewidth is $(1 + \alpha^2)$ times larger than the Shawlow–Townes fundamental limit. α is inversely proportional to the differential gain and it is evident that large differential gains are attainable in QD lasers. Therefore, low α-factors can be expected and have indeed been reported in conventional QD lasers [2]. We have measured the linewidth enhancement factor of the tunnel injection lasers by the Hakki–Paoli method at threshold by using the formula:

$$\alpha = \frac{2}{\partial\lambda} \frac{\Delta\lambda_i}{\Delta\{\ln[(\sqrt{r_i} - 1)(\sqrt{r_i} + 1)^{-1}]\}},$$

where $\partial\lambda$ is the mode spacing, r_i is the peak-to-averaged valleys ratio of the ith competing mode in the optical spectrum and ΔN is the incremental carrier density for two differential bias values [27]. It is worth noting that the subthreshold measurement results employed have shown excellent agreement with results from other measurements of α-factor above threshold, such as injection locking, in QW lasers [28]. The results of the two techniques may be different in QD lasers if these devices exhibit multi-mode lasing from the excited states at high biases [29]. However, spectral measurements of our lasers show a stable single-mode output spectrum from the ground state of QDs at all biases, and thus the subthreshold Hakki–Paoli technique should yield the true value of α. The sub-threshold spectra were measured under pulsed bias (10 kHz, 1%) at room temperature with a HP 70952B optical spectrum analyser with a minimum resolution of 0.8 Å. The voltage increment, ΔV, was kept below 0.1 V. The measured linewidth enhancement factors are shown against the peak wavelength of the subthreshold spectrum for the undoped TI 1.1 μm QD laser in figure 10(a). The value of α at lasing peak (~1057 nm) is ~0.73, which is lower than what is measured in conventional SCH QD lasers [2]. At other wavelengths, the value of α is $\leqslant 0.5$. This is an indication of reduced hot carrier densities in the tunnel injection laser. The reduction of α in QD lasers, compared to typical values >2 in QW lasers, implies a very small refractive index change in the lasing core. Consequently, there is a reduction of the self-focusing effect in these devices, which leads to absence of filamentation in their measured near-field pattern, as we have reported elsewhere [27].

As can be seen in figure 10(b), upon varying the voltage increment, ΔV, from a differential value of 0.1 V to values as high as 0.5 V, no spectral differential shift of the longitudinal laser peaks, $\Delta\lambda_i$, was observed in p-doped 1.1 μm TI lasers. Therefore, α is virtually zero in these lasers (within the resolution of our spectrum analyser). The α-factors of the 1.3 μm devices were measured by the same method and, similarly, the values of the α-factors are essentially zero versus wavelength around the lasing peak.

Finally, since chirp is directly proportional to α, tunnel injection QD lasers are expected to have ultra-low chirp. We measured the chirp in both 1.1 and 1.3 μm TI QD lasers from the difference in the linewidth of single longitudinal modes with and without superimposition of an ac signal. The envelope of the dynamic shift in wavelength of the sinusoidal modulation signal was recorded with an optical spectrum analyser. The evaluated chirp for the undoped 1.1 μm TI QD lasers versus peak-to-peak modulation current is shown in figure 11(a) at a modulation frequency of 5 GHz and dc bias of 28 mA. For comparison, the same figure presents our results from InGaAs 1.0 μm QW lasers, whose heterostructure design and device fabrication are similar to the TI QD lasers. The chirp of the QW lasers varies between 1.6 and 2.9 Å and is comparable to previously reported values [30], whereas the value is ~0.4 Å in the TI QD lasers. Furthermore, upon changing the modulation frequency from 1 to 15 GHz and at a constant ac bias of 36 mA,

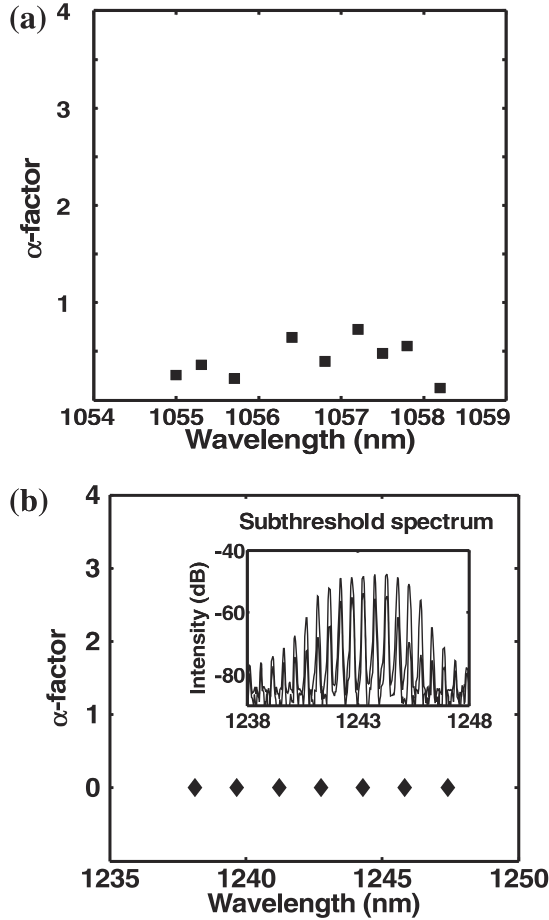

Figure 10. Linewidth enhancement factor at the peak wavelengths of the subthreshold spectrum of (*a*) undoped and (*b*) p-doped 1.1 μm tunnel injection QD lasers. The inset in (*b*) shows two differentially close measured subthreshold spectra with bias voltage difference, $\Delta V \sim 0.1$ V in the p-doped lasers.

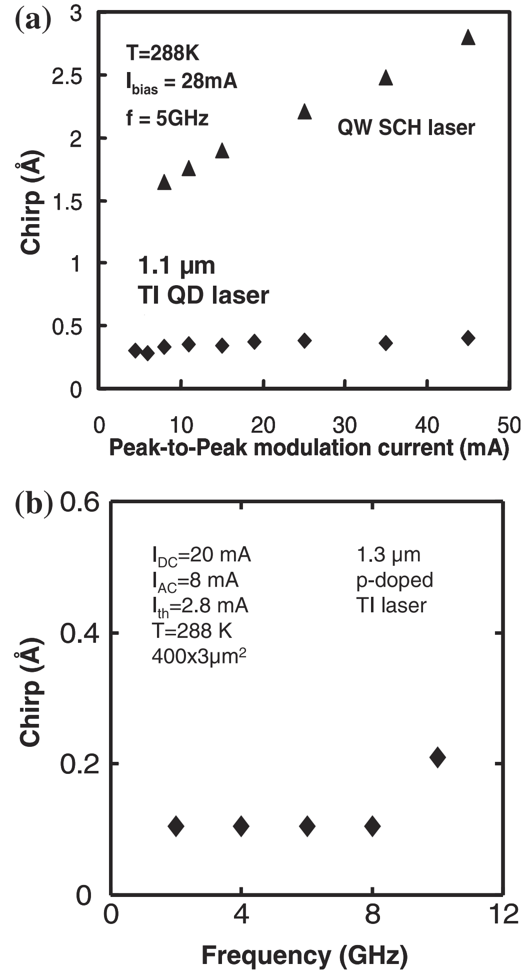

Figure 11. (*a*) Measured chirp for undoped 1.1 μm tunnel injection QD laser and SCH QW laser at different peak-to-peak modulation currents; (*b*) chirp versus modulating frequency in 1.3 μm p-doped tunnel injection QD lasers.

the TI QD lasers show chirp of <0.6 Å at all frequencies. The measured chirp in 1.3 μm lasers as a function of modulating frequency, with a peak-to-peak modulation current of 8 mA and a dc bias of 20 mA, is shown in figure 11(*b*). As can be seen, the dynamic chirp is negligible (<0.2 Å). Similar results were obtained for 1.1 μm tunnel injection QD lasers and are not discussed further herein. It can be clearly concluded that tunnel injection QD lasers have dynamic properties that surpass those of QW lasers for 1.0–1.3 μm optical communication systems.

8. Conclusions

The characteristics of very high performance 1.1 and 1.3 μm self-organized QD lasers are presented. The effects of tunnel injection and p-doping have been studied. While small-signal modulation bandwidths up to 11 GHz can be measured with p-doping alone, bandwidths up to 25 GHz are measured in tunnel injection lasers. The p-doped lasers demonstrate $T_0 = \infty$, together with near-zero chirp and α-factors.

Acknowledgments

This work is being supported by the US Army Research Office under Grant DAAD19-01-1-0331 and by the Center for Optoelectronic Nanostructures Semiconductor Technologies, a DARPA UPR award, under Contract HR0011-04-1-0040. The authors gratefully acknowledge Professor Siddhartha Ghosh and Dr Sameer Pradhan for their contribution and useful discussions.

References

[1] Eliseev P G, Li H, Liu T, Newell T C, Lester L F and Malloy K J 2001 *IEEE J. Selected Topics Quantum Electron.* **7** 135

[2] Newell T C, Bossert D J, Stintz A, Fuchs B, Malloy K and Lester L F 1999 *IEEE Photon. Technol. Lett.* **11** 1527

[3] Saito H, Nishi K, Kamei A and Sugou S 2000 *IEEE Photon. Technol. Lett.* **12** 1298

[4] Kamath K K, Phillips J, Jiang H, Singh J and Bhattacharya P 1997 *Appl. Phys. Lett.* **70** 2952

[5] Matthews D R, Summers H D, Smowton P M and Hopkinson M 2002 *Appl. Phys. Lett.* **81** 4904

[6] Bhattacharya P, Ghosh S, Pradhan S, Singh J, Wu Z-K, Urayama J, Kim K and Norris T B 2003 *IEEE J. Quantum Electron.* **39** 952

[7] Miyamoto Y, Miyake Y, Asada M and Suematsu Y 1989 *IEEE J. Quantum Electron.* **25** 2001

[8] Deppe D G, Huang H and Shchekin O B 2002 *IEEE J. Quantum Electron.* **38** 1587

[9] Shchekin O B, Ahn J and Deppe D G 2002 *Electron. Lett.* **38** 712

[10] Asryan L and Luryi S 2001 *IEEE J. Quantum Electron.* **37** 905

[11] Ghosh S, Pradhan S and Bhattacharya P 2002 *Appl. Phys. Lett.* **81** 3055

[12] Fathpour S, Chakrabarti S, Bhattacharya P, Kovsh A R, Mikhrin S S, Krestnikov I L, Kozhukhov A V and Ledentsov N N 2004 *Appl. Phys. Lett.* **85** 5164

[13] Fathpour S, Mi Z, Chakrabarti S, Bhattacharya P, Kovsh A R, Mikhrin S S, Krestnikov I L, Kozhukhov A V and Ledentsov N N 2004 *62nd Device Research Conf. Digest (Notre Dame, IN)* vol 62, p 156

[14] Urayama J, Norris T B, Jiang H, Singh J and Bhattacharya P 2002 *Appl. Phys. Lett.* **80** 2162

[15] Deppe D G and Huffaker D L 2000 *Appl. Phys. Lett*. **77** 3325

[16] Bhattacharya P, Singh J, Yoon H, Zhang X, Gutierrez-Aitken A and Yam L 1996 *IEEE J. Quantum Electron.* **32** 1620

[17] Zhang X, Gutierrez-Aitken A, Klotzkin D, Bhattacharya P, Caneau C and Bhat R 1997 *IEEE J. Selected Topics Quantum Electron.* **3** 309

[18] Yoon H, Gutierrez-Aitken A, Jambunathan R, Singh J and Bhattacharya P 1995 *IEEE Photon. Technol. Lett.* **7** 974

[19] Bhattacharya P and Ghosh S 2002 *Appl. Phys. Lett*. **80** 3482

[20] Vahala K J and Zah C E 1998 *Appl. Phys. Lett*. **52** 1945

[21] Uomi K 1990 *Japan. J. Appl. Phys*. **29** 81

[22] Gionannini M 2004 *Proc. SPIE Int. Soc. Opt. Eng*. **5452** 526

[23] Kim K, Urayama J, Norris T B, Singh J, Phillips J and Bhattacharya P 2002 *Appl. Phys. Lett.* **81** 670

[24] Kochman B, Stiff-Roberts A D, Chakrabarti S, Phillips J D, Krishna S, Singh J and Bhattacharya P 2001 *IEEE J. Quantum Electron.* **39** 459

[25] Ghosh S, Bhattacharya P, Stones E, Singh J, Jiang H, Nuttinck S and Laskar J 2001 *Appl. Phys. Lett*. **79** 722

[26] Marko I P, Andreev A D, Adams A R, Krebs R, Reithmaier J P and Forchel A 2003 *IEEE J. Selected Topics Quantum Electron.* **9** 1300

[27] Fathpour S, Bhattacharya P, Pradhan S and Ghosh S 2003 *Electron. Lett.* **39** 1443

[28] Liu G, Jin X and Chuang S L 2001 *IEEE Photon. Technol. Lett*. **13** 430

[29] Markus A, Chen J X, Gauthier-Lafaye O, Provost J-G, Paranthoën C and Fiorce A 2003 *IEEE J. Selected Topics Quantum Electron.* **9** 1308

[30] Saito H, Nishi N and Sugou S 2001 *Electron. Lett.* **37** 1293